



OPEN

Molybdenum sulfide modified with nickel or platinum nanoparticles as an effective catalyst for hydrogen evolution reaction

Mariusz Szkoda^{1,2}, Daria Roda¹, Malgorzata Skorupska³, Rafał Glazer¹ & Anna Ilnicka³

In this study, we investigate the catalytic performance of molybdenum sulfide (MoS₂) modified with either nickel (Ni) or platinum (Pt) nanoparticles as catalysts for the hydrogen evolution reaction (HER). The MoS₂ was prepared on the TiO₂ nanotube substrates via a facile hydrothermal method, followed by the deposition by magnetron sputtering of Ni or Pt nanoparticles on the MoS₂ surface. Structural and morphological characterization confirmed the successful incorporation of Ni or Pt nanoparticles onto the MoS₂ support. Electrochemical measurements revealed that Ni- and Pt-modified MoS₂ catalysts exhibited enhanced HER activity compared to pristine MoS₂. Obtained catalysts demonstrated a low onset potential, reduced overpotential, and increased current density, indicating efficient electrocatalytic performance. Furthermore, the Ni or Pt-modified MoS₂ catalyst exhibited remarkable stability during prolonged HER operation. The improved catalytic activity can be attributed to the synergistic effect between metal nanoparticles and MoS₂, facilitating charge transfer kinetics and promoting hydrogen adsorption and desorption. Incorporating Ni and Pt nanoparticles also provided additional active sites on the MoS₂ surface, enhancing the catalytic activity.

Keywords Catalytic performance, Molybdenum sulfide, Nickel and platinum nanoparticles, Hydrogen evolution reaction (HER), Synergistic effect

The hydrogen evolution reaction (HER) is crucial in various energy conversion and storage applications, including water splitting and fuel cells. Developing efficient and stable catalysts for HER is essential for advancing these technologies^{1–3}. Among the various catalyst materials explored, molybdenum sulfide (MoS₂) has gained significant attention due to its unique electronic structure, abundance, and cost-effectiveness^{4–7}.

MoS₂ possesses a layered structure composed of molybdenum (Mo) atoms sandwiched between sulfur (S) atoms, resulting in a catalytically active edge site that facilitates hydrogen adsorption and subsequent electrochemical reactions^{8,9}. However, pristine MoS₂ exhibits limitations in terms of its catalytic activity and stability^{10,11}. To overcome these challenges, researchers have explored the modification of MoS₂ with metal nanoparticles (Pt, Ag, Pd, Fe, Co, Cu) to enhance its catalytic properties for HER^{6,12–15}.

The incorporation of metal nanoparticles onto the MoS₂ surface can introduce additional active sites, alter the electronic structure, and enhance the charge transfer kinetics, thereby improving the catalytic performance for HER. The synergistic effect between the metal nanoparticles and MoS₂ is believed to be crucial in enhancing the overall catalytic activity^{14,15}.

Several studies have reported the modification of MoS₂ with metal nanoparticles and their influence on HER performance^{6,10}. For example, Lou et al. investigated the electrocatalytic activity of Pd-modified MoS₂ nanosheets and observed a significant reduction in the overpotential for HER compared to pristine MoS₂¹⁶. They attributed this improvement to the enhanced hydrogen adsorption on the active sites provided by the Pd nanoparticles. In another study, Bar-Ziv et al.¹⁷ explored the catalytic properties of Au-modified MoS₂ nanosheets. The Au

¹Faculty of Chemistry, Department of Chemistry and Technology of Functional Materials, Gdańsk University of Technology, Narutowicza 11/12, 80-233 Gdańsk, Poland. ²Advanced Materials Center, Gdańsk University of Technology, Narutowicza 11/12, 80-233 Gdańsk, Poland. ³Faculty of Chemistry, Nicolaus Copernicus University in Torun, Gagarina 7, 87-100 Toruń, Poland. ✉email: mariusz.szkoda1@pg.edu.pl

nanoparticles improved the catalytic activity and exhibited excellent stability during prolonged HER operation. The authors suggested that the Au nanoparticles facilitated charge transfer and enhanced the electrocatalytic performance of MoS₂. These findings demonstrate the potential of MoS₂ modification with metal nanoparticles for enhancing HER catalytic activity. However, further investigations are necessary to understand the underlying mechanisms and optimize the catalyst design for improved performance.

In this study, we aim to examine the catalytic performance of molybdenum sulfide catalysts modified with nickel (Ni) or platinum (Pt) nanoparticles for the hydrogen evolution reaction. The preparation of MoS₂-based catalysts involved a facile hydrothermal method of MoS₂ deposition on titanium dioxide (TiO₂) nanotube (NT) substrates, followed by deposition of Ni or Pt nanoparticles by magnetron sputtering. The role of TiO₂ in the system is integral, serving as a platform for the deposition of molybdenum disulfide (MoS₂). Specifically, the nanotubes of TiO₂ function as a porous and rough surface, facilitating the effective deposition of MoS₂. The porous and rough characteristics of TiO₂ nanotubes provide an advantageous substrate for MoS₂, significantly enhancing the system's catalytic performance. It is well-known that a catalyst's surface area is a desirable feature, as a larger surface area generally corresponds to improved catalytic activity. Additionally, TiO₂ is known for its excellent stability, which ensures the durability of the catalytic system over time^{18–21}. Extensive structural and morphological characterizations were performed to verify the successful incorporation of the metal nanoparticles onto the MoS₂ support. These characterizations provided essential evidence of the proper integration of Ni or Pt nanoparticles with the MoS₂ catalysts.

Experimental

TiO₂NT preparation

TiO₂ nanotubes were obtained by one-step anodization of titanium foil according to a procedure previously described in the literature²². The pre-cut pieces of titanium foil were cleaned using an ultrasonic bath in a mixture of isopropanol and acetone (1:1 vol.) for 30 min. Then, the anodization was performed in a two-electrode system in which both electrodes (anode and cathode) were titanium sheets. The electrolyte was a mixture of water and glycol in a volume ratio 1:19, 0.27 M ammonium fluoride, and 1 M phosphoric acid (V). The titanium electrodes were placed 2 cm from each other. The process of preparing nanotube structures on the anode was carried out for 2 h at a constant potential of 40 V using a programmable switching D.C. power supply PSB-2400L2, GW Instek. After anodization, the TiO₂ nanotubes layer was washed in a solution of 100 µl of HF in 50 cm³ of water, followed by distilled water. To transform the amorphous structure of the material into a crystalline form, it was annealed for 2 h at 450 °C in air at the end. Based on our previous reports^{23–25}, the diameter of the TiO₂ nanotubes obtained under these anodization parameters is approximately 100 nm, and their length is around 2 µm.

MoS₂ deposition on TiO₂NT

Layers of MoS₂ on TiO₂ nanotubes were deposited using a hydrothermal method. Table 1 presents the composition of the precursor solutions used to optimize the deposition process. TiO₂NT sheets were placed in the autoclave (volume 35 cm³) leaning against a wall at a 45° angle. In all cases, the autoclave contained 10 cm³ of precursor solution, and the process was carried out for 24 h at 240 °C. The resulting layers were washed in distilled water.

Preparation of hybrids TiO₂NT/MoS₂ with Ni and TiO₂NT/MoS₂ with Pt

In the experimental procedure, nickel (20 nm) was deposited onto crystalline TiO₂ nanotubes (TiO₂NT) or TiO₂NT/MoS₂ using magnetron sputtering. The sputtering process was conducted at room temperature, and three configurations were employed. The resulting samples were designated as follows: (I) TiO₂NT/MoS₂/Ni: In this configuration, nickel was sputtered directly onto the surface of TiO₂NT/MoS₂, forming a layer of nickel on top of the hybrid structure. (II) TiO₂NT/Ni/MoS₂: In this configuration, nickel was sputtered beneath a layer of MoS₂, with the deposition occurring on the TiO₂ nanotubes. This arrangement involved nickel being sandwiched between the TiO₂NT and the MoS₂ layer. (III) TiO₂NT/Ni/MoS₂/Ni: This configuration involved a deposition process similar to the previous configuration. Nickel was sputtered beneath a layer of MoS₂ on the TiO₂ nanotubes, and then an additional layer of nickel was sputtered on top of the MoS₂ layer.

Similarly, platinum (20 nm) was deposited onto the samples using magnetron sputtering, following the same experimental configurations as described earlier. The sputtering process was conducted at room temperature, ensuring precise control over the deposition process. The resulting samples were denoted based on the specific configurations: TiO₂NT/MoS₂/Pt, TiO₂NT/Pt/MoS₂, and TiO₂NT/Pt/MoS₂/Pt. The deposition of platinum and nickel in these configurations aims to assess the catalytic performance, electrochemical activity, and stability of the TiO₂NT/MoS₂ hybrid materials compared to the non-metal-containing configurations. By studying the effects of metals, a valuable understanding of their potential for electrocatalytic applications is gained. The schematic

No	Substrate 1	Concentration (mmol/dm ³)	Substrate 2	Concentration (mmol/dm ³)	Solvent
I	Na ₂ MoO ₄	28.6	Thiourea	142.9	Water
II	(NH ₄) ₂ MoS ₂	28.6	Thiourea	142.9	Water
III	(NH ₄) ₂ MoS ₂	28.6	–	–	Water
IV	(NH ₄)MoS ₂	28.6	–	–	DMF

Table 1. Composition of the precursor solutions.

representations of the different configurations are illustrated in Fig. 1. This figure showcases the various arrangements and layers of the materials, providing a visual reference to how the catalysts are obtained.

Materials characterization

Characterization of $\text{TiO}_2\text{NT}/\text{MoS}_2$

Figure 2 shows scanning electron microscopy (SEM) images of MoS_2 films obtained from precursor solutions of different compositions (Table 1). In all cases, except for the layer deposited from solution III, the entire surface of the substrate was covered. In the SEM image of the MoS_2 layer obtained from $(\text{NH}_4)_2\text{MoS}_2$ in water (solution

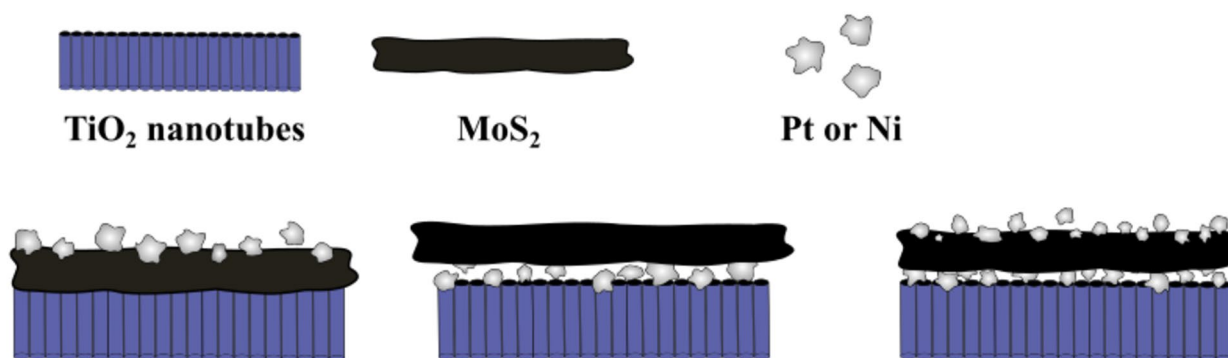


Figure 1. Schematic representations of the different configurations. The diagrams illustrated the layered structure and positioning of the components within the hybrid materials.

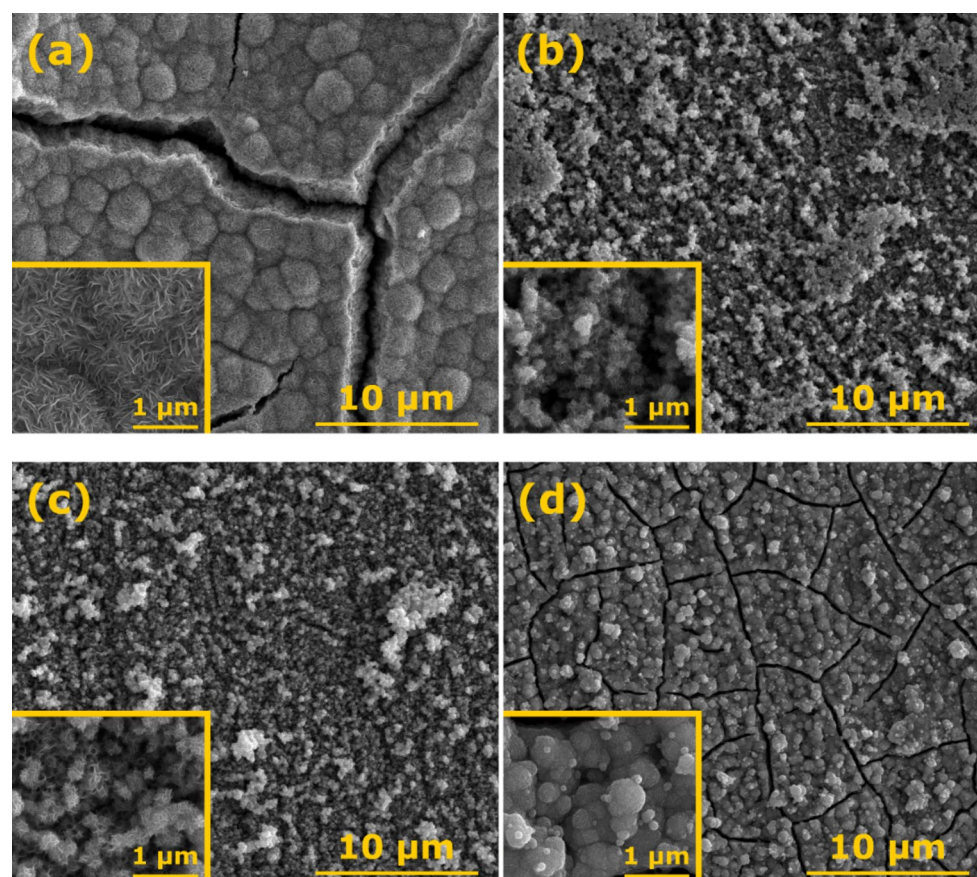


Figure 2. SEM images of $\text{TiO}_2\text{NT}/\text{MoS}_2$ materials obtained from (a) Na_2MoO_4 , thiourea, water; (b) $(\text{NH}_4)_2\text{MoS}_2$, thiourea, water; (c) $(\text{NH}_4)_2\text{MoS}_2$, water and (d) $(\text{NH}_4)_2\text{MoS}_2$, DMF.

III), the surface of TiO₂ nanotubes can be seen. The use of solutions I (NaMoO₄, thiourea, water) and solution IV ((NH₄)₂MoS₂, DMF) resulted in a smooth surface of the MoS₂ layers; however, cracks in the layer can be observed. A similar layer morphology was obtained from solution II ((NH₄)₂MoS₂, thiourea, water) and solution III ((NH₄)₂MoS₂, water). Despite some similarities, distinct differences in morphology can be observed depending on the raw material used. Each precursor follows a distinct chemical reaction pathway during hydrothermal synthesis. This affects the nucleation and growth rates of MoS₂ crystals. Different precursors create different pH and ionic environments during the hydrothermal process. These conditions influence the crystallinity and phase of the resulting MoS₂, leading to variations in morphology. For example, the use of Na₂MoO₄ might lead to a different ionic strength in the solution compared to (NH₄)₂MoS₂, impacting the growth dynamics of MoS₂. Moreover, the sulfur source in the precursor material plays a crucial role in the final structure of MoS₂. Thiourea and (NH₄)₂MoS₂ provide sulfur differently during the synthesis, impacting how sulfur atoms incorporate into the MoS₂ lattice, which in turn affects the morphology.

The obtained materials were further characterized using transmission electron microscopy (TEM). In the TEM images of TiO₂NT/MoS₂ at different magnifications (Fig. 3), similar to the SEM analysis, the TiO₂ nanotubes (TiO₂NT) are not visible. The powder used for analysis was scraped from the surface of the wafer, and only the top layer of MoS₂ crystals is observed in the images, without any indication of TiO₂ nanotubes.

Figure 4 shows a comparison of X-ray diffraction (XRD) patterns of layers obtained from precursor solutions of different compositions. The patterns of the layers obtained from solutions II, III, and IV contain peaks corresponding only to pure TiO₂ nanotubes. Only in the case of the layer obtained from the aqueous solution containing Na₂MoO₄ and thiourea (solution I) can be observed additional peaks at ~15° and 33°, which correspond

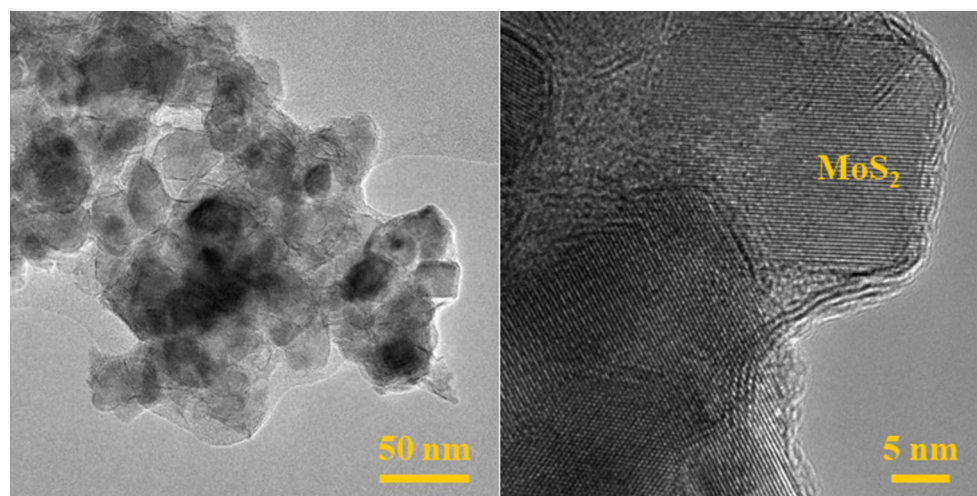


Figure 3. TEM images of TiO₂NT/MoS₂ with different magnifications.

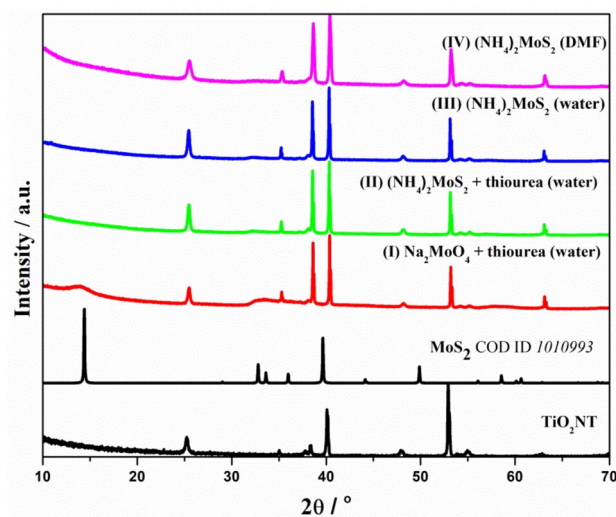


Figure 4. XRD patterns TiO₂NT/MoS₂ materials obtained from Na₂MoO₄, thiourea, water; (NH₄)₂MoS₂, thiourea, water; (NH₄)₂MoS₂, water and (NH₄)₂MoS₂, DMF.

to the (002) and (100) planes of MoS_2 , respectively. Using the XRD technique, it was impossible to confirm the deposition of MoS_2 from II, III, and IV solutions. This is related to the fact that the layers were obtained in amorphous form, as no peaks are visible except those from TiO_2NT .

The elemental mapping (Fig. 5) confirmed the presence of Mo and S on the entire surface of the electrodes studied. When solutions I and IV were used, Mo and S were distributed more uniformly over the entire surface than in the case of solutions II and III layers. In the images of the layers from solutions II and III, areas of increased Mo and S can be observed, and it is worth noting that areas of increased Mo correspond with those where more S can be seen. This indicates the presence of a compound containing both Mo and S, such as MoS_2 . Table 2 shows the composition of each layer. Assuming that we obtained MoS_2 on TiO_2 nanotubes, the layers from solutions III and IV were characterized by an excess of Mo and O, which may indicate the formation of molybdenum oxides. A slight excess of Ti can be observed in the layers from solutions I and II; however, these responses are from the substrate, as the nanotubes were obtained directly on the titanium sheet.

Electrochemical characterization of $\text{TiO}_2\text{NT}/\text{MoS}_2$

The obtained materials were tested as electrodes for electrocatalytic hydrogen evolution. Figure 6a shows a comparison of the linear sweep voltammetry (LSV) curves of the electrodes at a scanning rate of 5 mV s^{-1} . As can be observed in the inset of Fig. 6a, the material obtained from a solution containing Na_2MoO_4 with thiourea

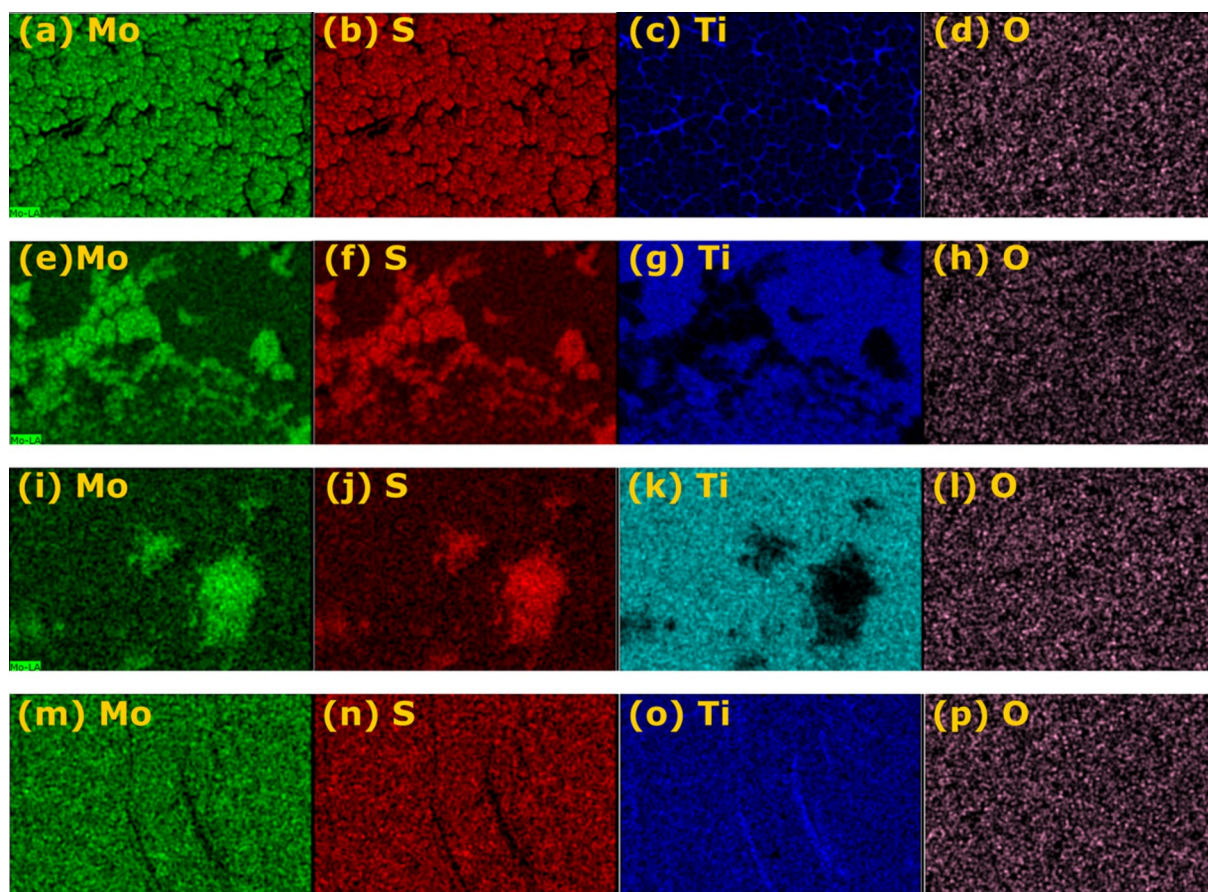


Figure 5. EDX elemental maps for Mo, S, Ti, and O of $\text{TiO}_2\text{NT}/\text{MoS}_2$ materials obtained from (a–d) Na_2MoO_4 , thiourea, water; (e–h) $(\text{NH}_4)_2\text{MoS}_2$, thiourea, water; (i–l) $(\text{NH}_4)_2\text{MoS}_2$, water and (m–p) $(\text{NH}_4)_2\text{MoS}_2$, DMF.

Sample	Mass percent (%)				
	C	Mo	S	Ti	O
(I) NaMoO_4 + thiourea (water)	0.38	52.18	22.94	19.87	4.63
(II) $(\text{NH}_4)_2\text{MoS}_2$ + thiourea (water)	0.30	29.47	13.59	48.17	8.47
(III) $(\text{NH}_4)_2\text{MoS}_2$ (water)	0.89	16.43	7.92	29.20	45.56
(IV) $(\text{NH}_4)_2\text{MoS}_2$ (DMF)	0.58	5.80	4.89	37.63	51.10

Table 2. Layers composition determined by EDX analysis.

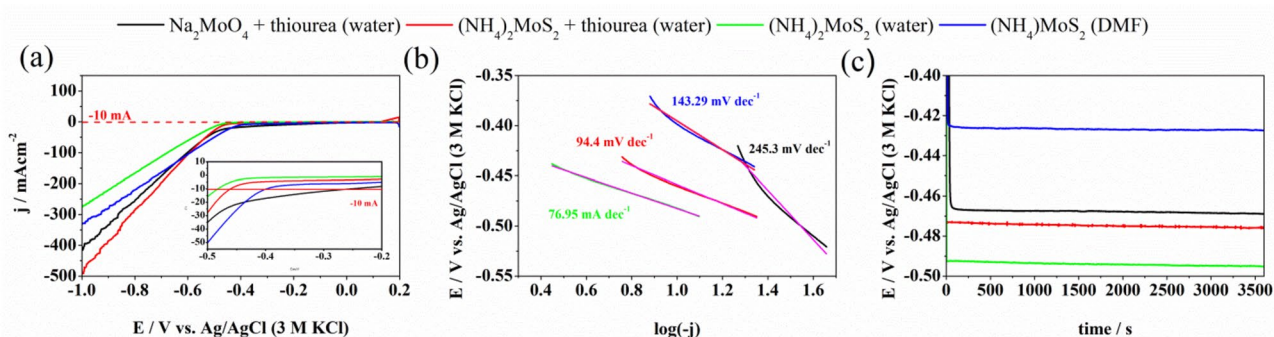


Figure 6. (a) LSV curves of $\text{TiO}_2\text{NT}/\text{MoS}_2$ electrodes obtained from different precursor solutions; inset: zooms of LSV curves from -0.5 to -0.2 V, (b) corresponding Tafel slopes, (c) chronopotentiometry curves of $\text{TiO}_2\text{NT}/\text{MoS}_2$ electrodes obtained from different precursors at the current density of 10 mA cm^{-2} .

in water (I) had the lowest overpotential at a current density of -10 mA cm^{-2} . However, the overpotentials for the other electrodes at this current density were very similar. A comparison of the Tafel slopes of $\text{TiO}_2\text{NT}/\text{MoS}_2$ electrodes is shown in Fig. 6b. The calculated slopes indicate that, according to the general HER model, the charge transfer step (Volmer reaction) is the step that determines the rate of the whole reaction²⁶. Layers deposited from solution III ($(\text{NH}_4)_2\text{MoS}_2$ in water) had the smallest Tafel slope and thus also the lowest exchange current density. The stability of the electrodes was also tested by applying a current density of -10 mA cm^{-2} for 1 h. As shown in Fig. 6c at 1 h, the potential of neither electrode changed significantly. Despite the highest hydrogen evolution overpotential, layers obtained from solution III were chosen for further study. The differences in the overpotentials of the electrodes were insignificant, and the electrode obtained by deposition from an aqueous solution of $(\text{NH}_4)_2\text{MoS}_2$ had the most preferable Tafel slope. The chosen synthesis was based on only one compound, without the need to add an additional sulfur precursor. The use of organic solvents was also avoided.

Characterization of hybrids $\text{TiO}_2\text{NT}/\text{MoS}_2$ with Ni and $\text{TiO}_2\text{NT}/\text{MoS}_2$ with Pt

The morphology of the obtained nickel and platinum-doped materials was determined by scanning electron microscopy analysis. The top part of Fig. 7 shows the SEM images of the synthesized hybrids of $\text{TiO}_2\text{NT}/\text{MoS}_2$ with Ni, and the bottom part of Fig. 7 presents hybrid images of $\text{TiO}_2\text{NT}/\text{MoS}_2$ with Pt at the different configurations of Ni and Pt positions. The as-received MoS_2 particles are irregular, with the majority having a size of 170 nm. The SEM images show that the distribution of MoS_2 particles is relatively homogenous, indicating that

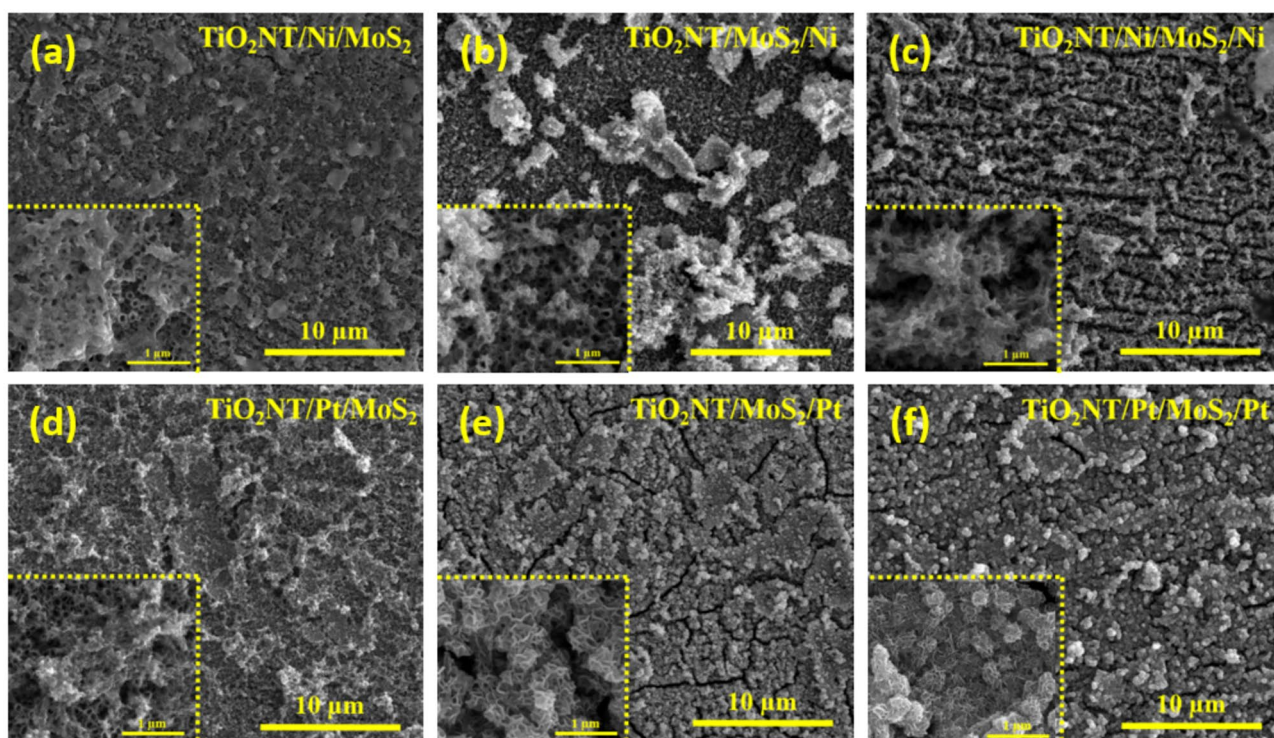


Figure 7. SEM images of hybrids $\text{TiO}_2\text{NT}/\text{MoS}_2$ with (a–c) Ni and (d–f) Pt at three different configurations.

the synthesis process facilitated a uniform dispersion of the particles on the TiO₂NT surface. The dense distribution of MoS₂ particles suggests a strong interaction between the MoS₂ and TiO₂NT, which is favorable for the desired properties and performance of the hybrid material. In the case of hybrid samples containing nickel, the MoS₂ layers structure is more connected and contains only thin ends in some places. In addition, many nodular agglomerated grains are seen on the hybrids with nickel-coating surfaces (TiO₂NT/MoS₂/Ni and TiO₂NT/Ni/MoS₂/Ni). For hybrid samples synthesized with platinum in the case of two TiO₂NT/MoS₂/Pt and TiO₂NT/Pt/MoS₂/Pt samples, where the platinum particles coat the surface of MoS₂, their structure is significantly different from the TiO₂NT/Pt/MoS₂ sample, where the platinum is only located under the MoS₂. The platinum causes the formation of rough and broader ends of MoS₂ with a number of small debris pieces. This phenomenon is not visible for TiO₂NT/Pt/MoS₂ where ends of the surface MoS₂ are thinner with no visible thickening and corrugations.

A detailed examination using transmission electron microscopy (TEM) revealed that the MoS₂ walls are composed of multiple layers distributed throughout the sample volume. The hybrid TiO₂NT/MoS₂/Ni (Fig. 8a,b) contains nickel particles dispersed irregularly across the structure. In the hybrid TiO₂NT/MoS₂/Pt (Fig. 8c,d), the presence of platinum metal is confirmed, with the platinum particles showing a tendency to agglomerate into larger clusters at several locations within the sample.

Energy dispersive X-ray (EDX) analysis was performed on two materials, TiO₂NT/Ni/MoS₂/Ni and TiO₂NT/Pt/MoS₂/Pt, to determine their elemental composition. The measurements were conducted at various locations on the samples to ensure representative results. The EDX analysis confirmed the presence of platinum, nickel, molybdenum, sulfur, titanium, and oxygen in both materials. The presence of nickel and platinum in TiO₂NT/Ni/MoS₂/Ni and TiO₂NT/Pt/MoS₂/Pt (Fig. 9), respectively, is consistent with the intended design and synthesis of these hybrids. The incorporation of molybdenum and sulfur can be attributed to the presence of MoS₂, while titanium and oxygen are inherent to the TiO₂NT substrate. These findings validate the successful integration of the desired elements into the hybrid structures. Importantly, the EDX analysis was conducted at multiple locations on the samples, ensuring that any potential variations in composition across the material were taken into account. The results indicate no significant differences in the quantity or distribution of the materials based on

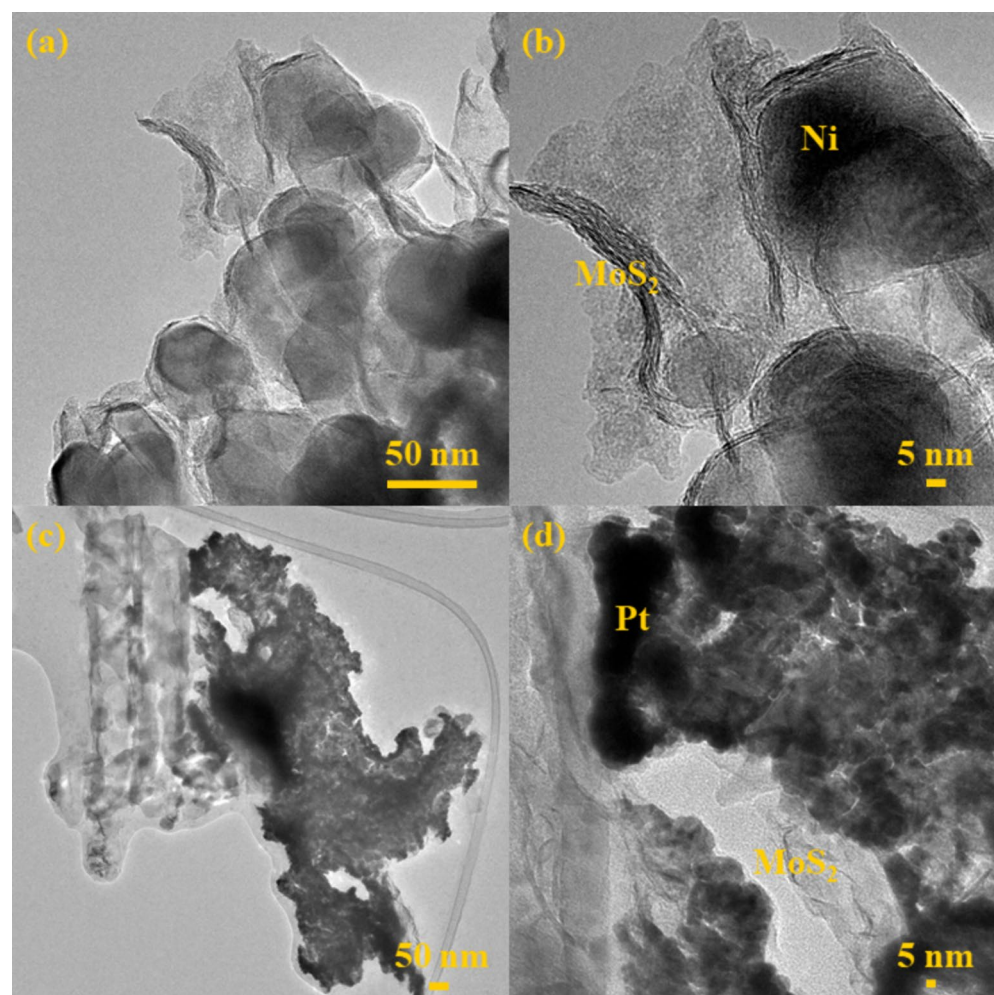


Figure 8. TEM images of (a, b) TiO₂NT/MoS₂/Ni and (c, d) TiO₂NT/MoS₂/Pt with different magnifications.

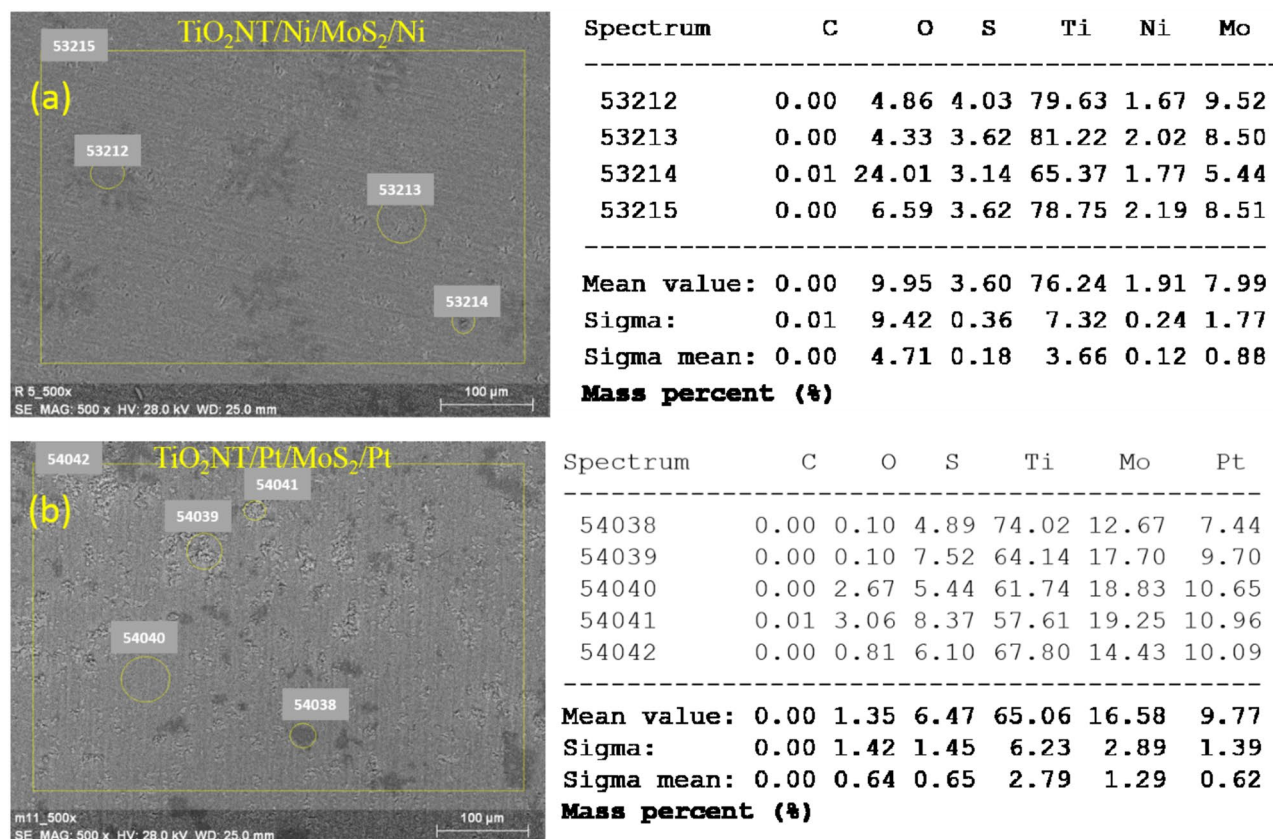


Figure 9. EDX spectra of (a) $\text{TiO}_2\text{NT}/\text{Ni}/\text{MoS}_2/\text{Ni}$ and (b) $\text{TiO}_2\text{NT}/\text{Pt}/\text{MoS}_2/\text{Pt}$.

the location of the sample. This uniformity in composition further supports the successful synthesis and uniform distribution of the elements within the $\text{TiO}_2\text{NT}/\text{Ni}/\text{MoS}_2/\text{Ni}$ and $\text{TiO}_2\text{NT}/\text{Pt}/\text{MoS}_2/\text{Pt}$ hybrid structures.

The XRD results were obtained for the $\text{TiO}_2\text{NT}/\text{MoS}_2$ hybrids with the inclusion of platinum or nickel in different configurations, as depicted in Fig. 10. The positions and intensities of dominant peaks corresponded well with the known crystallographic data for TiO_2 , confirming the presence of TiO_2 in the hybrid structures and crystalline nature of the substrate. Regarding MoS_2 , due to its amorphous nature, characteristic peaks corresponding to MoS_2 crystal lattice planes were not observed in the XRD patterns. This suggests the MoS_2 component might exist in a disordered or poorly crystalline state. However, it is worth noting that the XRD results did show some additional broadening or slight shifts in the TiO_2 peaks when comparing the different configurations of Pt or Ni. This could be indicative of interactions between the TiO_2 substrate and the Pt or Ni dopants, potentially affecting the crystalline structure or lattice parameters of TiO_2 . Additionally, the remaining diffraction peaks that were not assigned to TiO_2 likely originate from metallic titanium, corresponding to the substrate material²⁷.

Due to the lack of clear XRD peaks from MoS_2 in the obtained results, an additional investigative method, X-ray Photoelectron Spectroscopy (XPS), was employed to confirm the presence of MoS_2 in the samples.

To confirm the presence of molybdenum disulfide, nickel, and platinum, X-ray Photoelectron Spectroscopy measurements were conducted for three selected samples, pristine $\text{TiO}_2\text{NT}/\text{MoS}_2$ material and their hybrid with the addition of nickel $\text{TiO}_2\text{NT}/\text{Ni}/\text{MoS}_2/\text{Ni}$ and the addition of platinum $\text{TiO}_2\text{NT}/\text{Pt}/\text{MoS}_2/\text{Pt}$. Figures 11, 12 and 13 shows spectra for the Mo 3d, S 2p, O 1s, Ni 2p, and Pt 4f regions. The spectrum in the Mo 3d region (Figs. 11a, 12a, 13a) was fitted with four doublets ($d_{5/2}$ – $d_{3/2}$ separation of 3.13 eV), with the first main line of $3d_{5/2}$ at a binding energy of 228.6 eV, indicating the presence of molybdenum sulfide in the 1T phase. The second line of $3d_{5/2}$ at a binding energy of 229.1 eV suggests the presence of molybdenum sulfide in the 2H phase²⁸. The third line of $3d_{5/2}$ at a binding energy of 230.2 eV indicates the presence of molybdenum(IV) oxide, and the last line of $3d_{5/2}$ at a binding energy of 232.3 eV points to the presence of molybdenum(VI) oxide (MoO_3)²⁹.

An additional line at around 226 eV in binding energy originates from the S 2s line. The S 2p spectra (Figs. 11b, 12b, 13b) were fitted with three doublets ($p_{3/2}$ – $p_{1/2}$ separation of 1.16 eV), with the first main line of $2p_{3/2}$ at a binding energy of 161.5 eV, indicating the presence of sulfur in molybdenum sulfide in the 1T phase. The second line of $2p_{3/2}$ at a binding energy of 163.2 eV indicates the presence of sulfur in molybdenum sulfide in the 2H phase. The last line of $2p_{3/2}$ at a binding energy of 168.8 eV signifies the presence of sulfur in sulfate (VI)^{28,30}.

The spectra in the oxygen region (Figs. 11c, 12c, 13c) were fitted with three peaks. The first peak, located at an energy of 530.5 eV, corresponds to the presence of X–O bonds (where X = Mo, Ni, S or Ti). The second peak, at a binding energy of 532.0 eV, indicates the presence of both metal oxides (oxygen in non-stoichiometric oxides), organic groups such as O=C, and bonds such as O–S. The third peak, located at 533.5 eV, indicates the presence of bonds such as O–C and/or –OH^{31,32}. The spectrum in the nickel $2p_{3/2}$ region (Fig. 12d) was fitted with five lines. The first line, located at a binding energy of 856.6 eV, indicates the presence of nickel in the + 2 oxidation

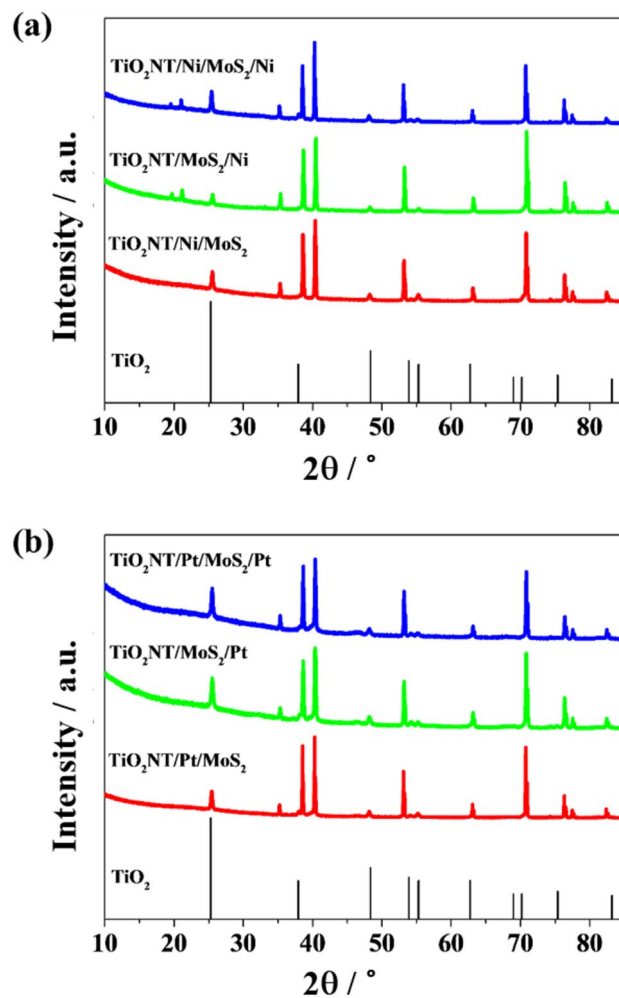


Figure 10. XRD patterns of hybrids $\text{TiO}_2\text{NT}/\text{MoS}_2$ with (a) Ni and (b) Pt at three different configurations were compared.

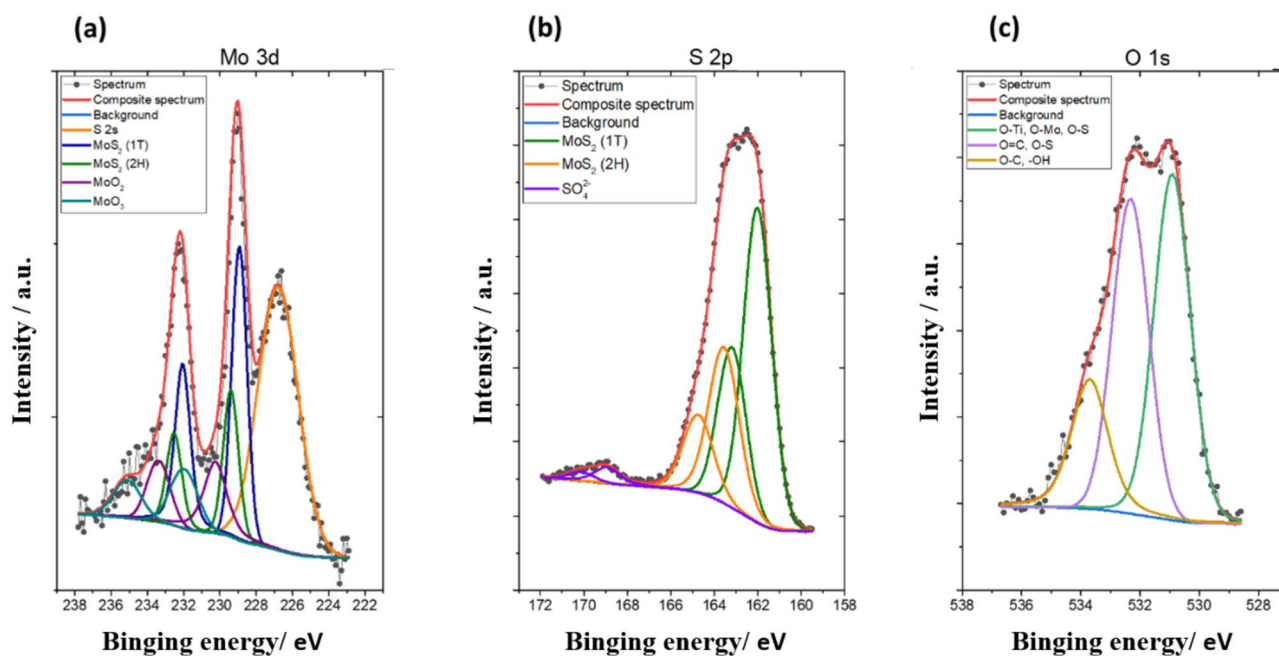


Figure 11. High-resolution XPS spectrum of (a) Mo 3d, (b) S 2p, and (c) O 1s of $\text{TiO}_2\text{NT}/\text{MoS}_2$.

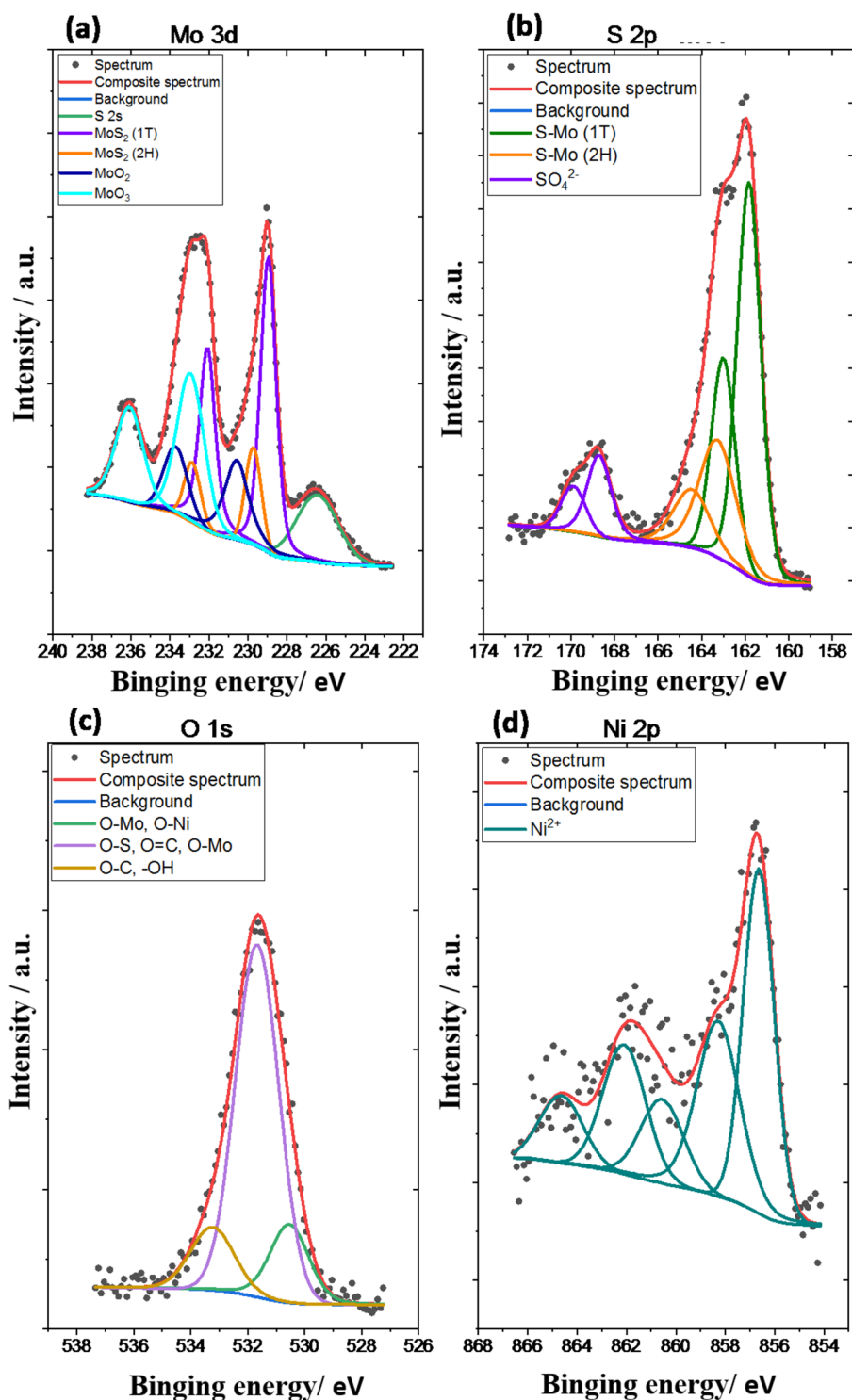


Figure 12. High-resolution XPS spectrum of (a) Mo 3d, (b) S 2p, (c) O 1s, and (d) Ni 2p of TiO₂NT/Ni/MoS₂/Ni.

state in oxide or hydroxide compounds³³. The remaining lines in the binding energy range of 858 to 865 eV are associated with multiplet splitting effects and further confirm the + 2 oxidation state of nickel. The spectrum in the Pt 4f region (Fig. 13d) was fitted with a doublet (the $f_{7/2}$ - $f_{5/2}$ separation is 3.33 eV) with the main $4f_{7/2}$ line lying at a binding energy of 71.2 eV indicating the presence of platinum metal³⁴.

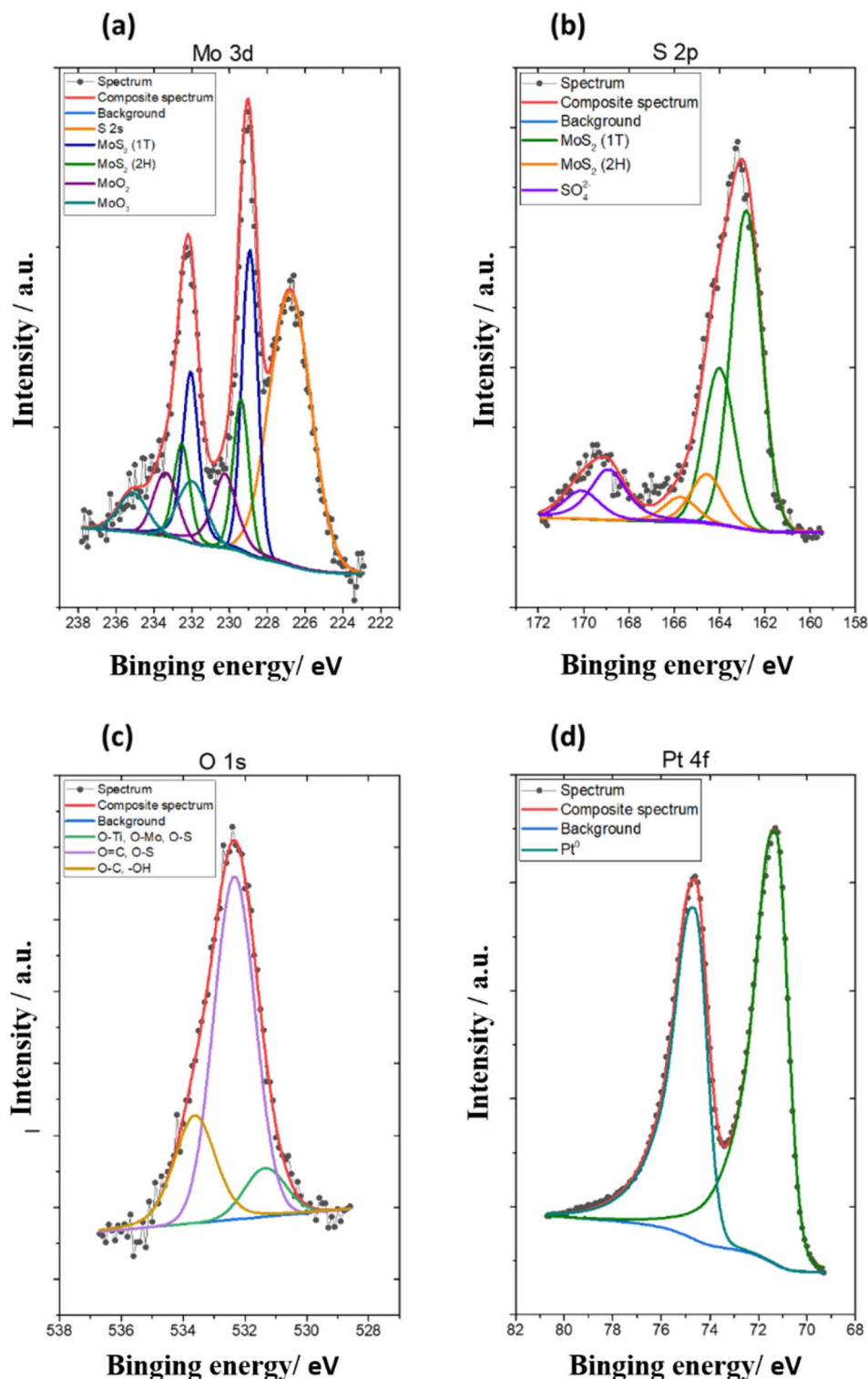


Figure 13. High-resolution XPS spectrum of (a) Mo 3d, (b) S 2p, (c) O 1s, and (d) Pt 4f of TiO₂NT/MoS₂/Pt.

Electrochemical performance of hybrids TiO₂NT/MoS₂ with Ni and TiO₂NT/MoS₂ with Pt

The hybrids obtained in this study were evaluated for their catalytic performance in the hydrogen evolution reaction under specific conditions. The measurements were conducted in a 0.2 M H₂SO₄ electrolyte using a three-electrode setup, employing a scan rate of 5 mV s⁻¹. To facilitate comparison, we also tested bare TiO₂ nanotubes and Pt as reference materials. The HER polarization curves of the commercial Pt and Ni discs, pure TiO₂ nanotubes, and the hybrids obtained in this study, both with and without the addition of metal, are presented in Fig. 14. The obtained hybrids exhibited promising catalytic activity for the hydrogen evolution reaction, as evident from the

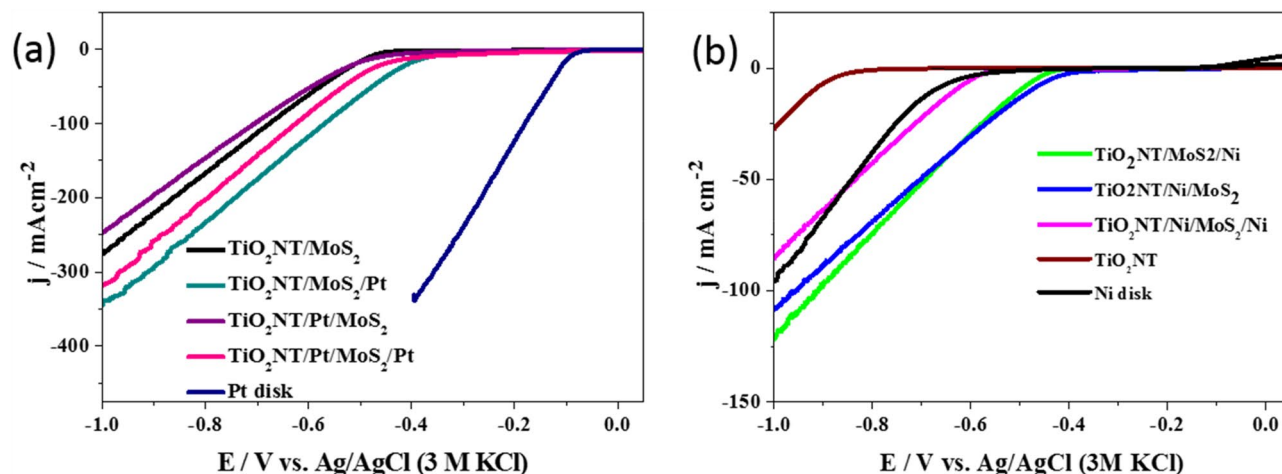


Figure 14. LSV curves (HER reaction) of hybrids $\text{TiO}_2\text{NT}/\text{MoS}_2$ with (a) Pt and (b) Ni in 0.2 M H_2SO_4 .

linear sweep voltammograms shown in Fig. 14a,b. However, it is worth noting that the overpotential values for achieving a current density of $j_{\text{HER}} = 10 \text{ mA cm}^{-2}$ were lower for the commercial Pt disc electrode compared to the hybrids but better than those observed for the commercial Ni disc electrode. This observation is summarized in Table 3, which presents the overpotential values for all the tested electrodes. Despite the slightly higher overpotential values, it is noteworthy that incorporating a small amount of metal resulted in an improvement of the hydrogen evolution overpotential compared to the TiO_2 nanotubes/ MoS_2 electrode (see Fig. 7, Table 3). This suggests that the addition of the metal component positively influenced the catalytic performance of the hybrids.

However, a phenomenon occurred where the $\text{TiO}_2\text{NT}/\text{Pt}/\text{MoS}_2/\text{Pt}$ configuration, with a higher quantity of platinum, exhibits poorer HER performance compared to than the $\text{TiO}_2\text{NT}/\text{MoS}_2/\text{Pt}$ configuration. This discrepancy can potentially be attributed to the intricate synergy between TiO_2NT and MoS_2 . One plausible hypothesis arises from the examination of $\text{TiO}_2\text{NT}/\text{Pt}/\text{MoS}_2$ and $\text{TiO}_2\text{NT}/\text{MoS}_2$ configurations. In these cases, the composite with platinum demonstrated lower catalytic activity compared to the platinum-free composite. It suggests that the presence of platinum between the layers of semiconductor materials has a detrimental effect on the catalytic activity of the composite. The negative impact of platinum presence between TiO_2NT and MoS_2 layers could be elucidated through various factors: (1) Platinum may disrupt the synergistic effects between TiO_2NT and MoS_2 . The optimal interaction between TiO_2NT and MoS_2 , crucial for enhanced catalytic activity, might be compromised by the introduction of platinum between them. (2) The presence of platinum could alter the charge transfer dynamics between TiO_2NT and MoS_2 , influencing the electron flow required for the hydrogen evolution reaction negatively. (3) Platinum nanoparticles may physically block active sites on either TiO_2NT or MoS_2 , hindering the accessibility of reactants and affecting the overall catalytic efficiency. Moreover, a similar phenomenon can be observed when nickel is used instead of platinum. In this case, when nickel is between the layers, the composites exhibit inferior activity, suggesting that the introduction of nickel between TiO_2NT and MoS_2 layers may also disrupt the balance and synergies, akin to the observed effects with platinum. Overall, while the obtained results were favorable, it is important to acknowledge that the catalytic activity of the hybrids, although enhanced by the presence of metal, still fell short of the performance exhibited by the commercial Pt disc electrode. However, utilizing a small amount of platinum and nickel in the hybrids offers a significant advantage in terms of cost-effectiveness. The cost of platinum, in particular, is relatively high, and its extensive use in industrial applications may not always be economically viable. By incorporating only a small quantity of these precious metals, the hybrids become a more practical and cost-effective alternative.

Electrode	Overpotential (mV) to achieve a current density of -10 mA cm^{-2}	Onset potential (mV)	b (mV dec^{-1})
$\text{TiO}_2\text{NT}/\text{MoS}_2$	484	459	77
$\text{TiO}_2\text{NT}/\text{MoS}_2/\text{Pt}$	366	370	159
$\text{TiO}_2\text{NT}/\text{Pt}/\text{MoS}_2$	462	488	185
$\text{TiO}_2\text{NT}/\text{Pt}/\text{MoS}_2/\text{Pt}$	388	437	276
Pt disk	98	82	38
Ni disk	676	678	171
$\text{TiO}_2\text{NT}/\text{MoS}_2/\text{Ni}$	503	459	63
$\text{TiO}_2\text{NT}/\text{Ni}/\text{MoS}_2$	476	425	137
$\text{TiO}_2\text{NT}/\text{Ni}/\text{MoS}_2/\text{Ni}$	634	592	63
TiO_2NT	926	872	229

Table 3. Electrochemical parameters determined from LSV curves and Tafel plots.

Impedance spectra obtained for TiO_2NT , $\text{TiO}_2\text{NT}/\text{Ni}/\text{MoS}_2$, $\text{TiO}_2\text{NT}/\text{Pt}$, $\text{TiO}_2\text{NT}/\text{MoS}_2/\text{Ni}$, $\text{TiO}_2\text{NT}/\text{MoS}_2/\text{Pt}$, $\text{TiO}_2\text{NT}/\text{MoS}_2$ are presented in Fig. 15. EIS spectra were taken at an onset potential for unmodified and modified electrodes. In each case where the metal was located on the outer layer, it was observed that these materials exhibited significantly lower charge transfer resistance compared to the other materials. Furthermore, the Nyquist plots for these materials showed a steeper slope, indicating more capacitive behaviour. The EIS results clearly show a noticeable improvement in electron transfer properties upon depositing the metal on the MoS_2 surface. The lower charge transfer resistance observed in $\text{TiO}_2\text{NT}/\text{MoS}_2/\text{Ni}$ and $\text{TiO}_2\text{NT}/\text{MoS}_2/\text{Pt}$ indicates a more efficient electron transfer process, which is crucial for catalytic applications such as HER. Additionally, the steeper slope in the Nyquist plot suggests a more capacitive nature, indicating an increased electrochemical surface area and availability of active sites. Interestingly, when the metal is located between TiO_2 and MoS_2 , higher charge transfer resistance was observed in the EIS curve. This higher value indicates a relatively lower electron transfer rate in the material, suggesting limited electrocatalytic activity. These studies confirm the hypotheses (1), (2) and (3) mentioned above regarding the reasons for poorer HER performance for materials where the metal was located between the layers.

Figure 16 illustrates the Tafel plots of hybrids $\text{TiO}_2\text{NT}/\text{MoS}_2$ with Pt and hybrids $\text{TiO}_2\text{NT}/\text{MoS}_2$ with Ni, which provide valuable insights into the kinetic behavior of the electrodes during the hydrogen evolution reaction. At high overpotentials, the HER is primarily kinetically controlled, and its behavior can be described by the Tafel equation:

$$\eta = a + b \log j$$

here η (V) represents the overpotential, a (V) corresponds to the cathodic intercept associated with the exchange current density, b (V dec^{-1}) represents the cathodic Tafel slope, and j (A cm^{-2}) denotes the catalytic current density. By analyzing the linear portion of the potential versus the logarithmic value of the current density, it becomes possible to calculate the Tafel slope values, which provide essential kinetic metrics of the catalyst.

These Tafel slope values offer valuable information about the electrocatalytic activity of the tested electrodes. They indicate the rate at which the catalytic current density changes with variations in the overpotential. The magnitude of the Tafel slope provides insights into the reaction mechanism and the effectiveness of the catalyst in promoting the desired electrochemical process. The Tafel plots reveal interesting trends among the tested hybrids containing different metals. It is observed that almost all the hybrids incorporating metals exhibited lower Tafel slopes compared to the pure TiO_2 nanotubes. This indicates a more efficient catalytic performance for the hybrids, as smaller Tafel slopes correspond to faster kinetics and better electrocatalytic activity. Notably, the hybrids with the addition of nickel stood out with significantly reduced Tafel slopes. These hybrids displayed a Tafel slope of 63 mV dec^{-1} , whereas the commercial Pt disc electrode exhibited a Tafel slope of 38 mV dec^{-1} , and the pure TiO_2 nanotubes demonstrated a much higher Tafel slope of 229 mV dec^{-1} . It is worth noting that

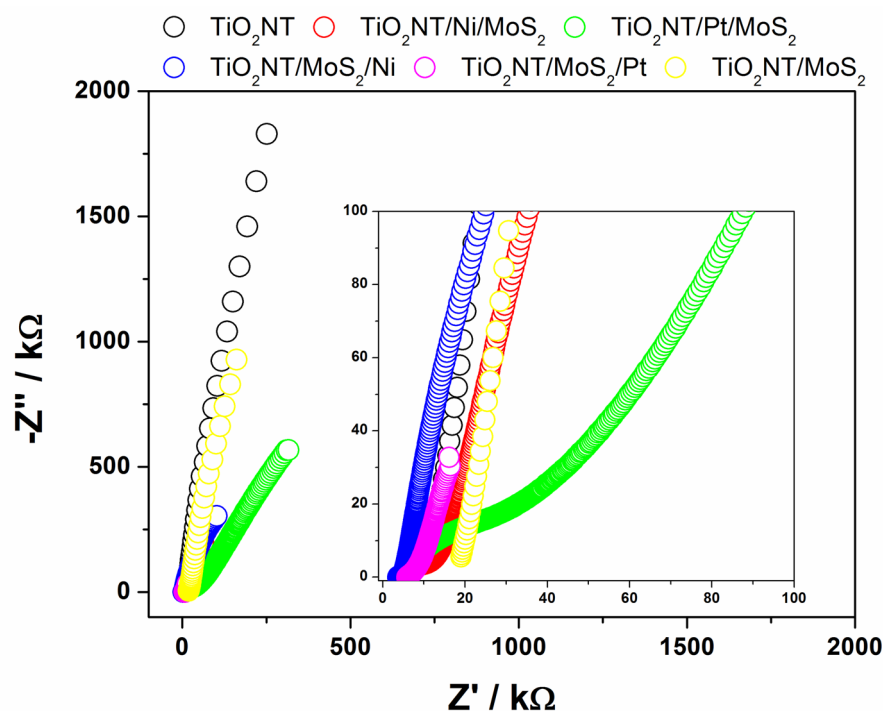


Figure 15. EIS spectra of obtained catalysts: TiO_2NT , $\text{TiO}_2\text{NT}/\text{Ni}/\text{MoS}_2$, $\text{TiO}_2\text{NT}/\text{Pt}$, $\text{TiO}_2\text{NT}/\text{MoS}_2/\text{Ni}$, $\text{TiO}_2\text{NT}/\text{MoS}_2/\text{Pt}$, $\text{TiO}_2\text{NT}/\text{MoS}_2$.

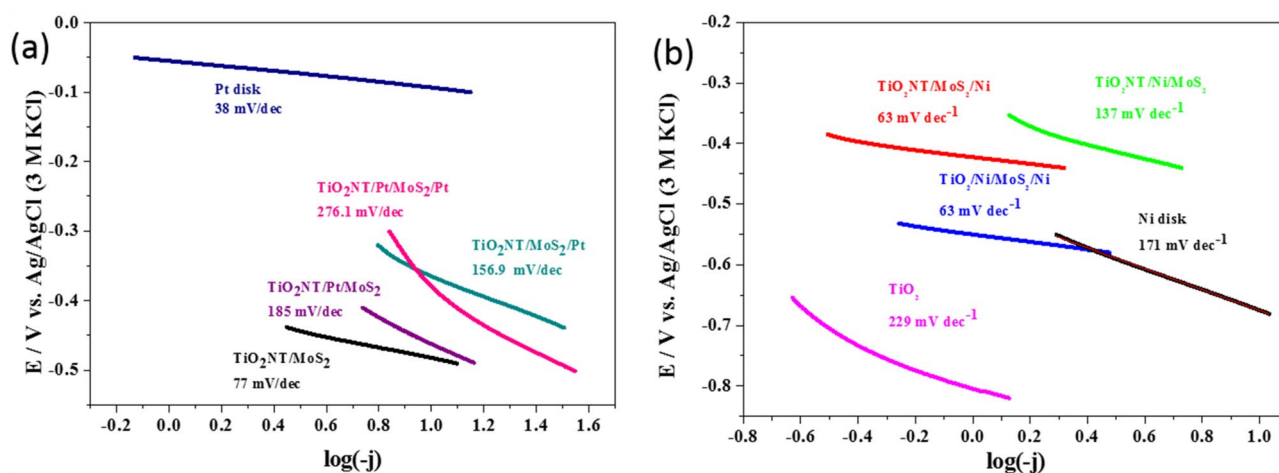


Figure 16. Tafel plots of hybrids $\text{TiO}_2\text{NT}/\text{MoS}_2$ with (a) Pt and (b) Ni determined from LSV in $0.2 \text{ M H}_2\text{SO}_4$.

the measured Tafel slope for the Ni disc was 171 mV dec^{-1} . This finding is particularly noteworthy because a lower Tafel slope signifies a higher catalytic reaction rate and improved performance in the hydrogen evolution reaction. Comparatively, the commercial Pt disc electrode, which serves as a benchmark due to its excellent catalytic activity, exhibits a lower Tafel slope of 38 mV dec^{-1} . However, it is noteworthy that the hybrids with the addition of nickel approached this level of performance, showcasing their potential as cost-effective alternatives to the platinum-based catalysts. Overall, these findings highlight the superiority of the hybrids containing metal additives, particularly nickel, in terms of their electrocatalytic performance. Furthermore, an interesting trend was observed regarding the positioning of the metal within the hybrids. It was noticed that when the metal was located on the surface of the MoS_2 rather than beneath it, the resulting hybrids exhibited superior catalytic performance. This observation suggests that the proximity of the metal to the active sites of MoS_2 plays a crucial role in enhancing the electrocatalytic activity. Placing the metal on the surface of MoS_2 facilitates better electron transfer and promotes synergistic effects between the metal and the MoS_2 , leading to improved catalytic efficiency in the hydrogen evolution reaction. The trend of surface positioning of the metal as a contributing factor to enhanced performance provides valuable insights for designing and developing efficient electrocatalysts. By strategically controlling the arrangement of metal and MoS_2 , it becomes possible to optimize the catalytic properties and achieve superior performance in various electrochemical processes. To compare the catalytic performance of the tested materials, the Tafel slope values were compiled and tabulated in Table 3.

In Table 4, literature-based Tafel slope results for MoS_2 -based materials are presented. As observed, some of the catalysts synthesized in this work fall within the range of values reported in the literature.

This consistency with literature values suggests that the electrocatalytic performance of the developed catalysts aligns with the trends and characteristics observed in prior research. The comparison provides additional validation and context for the obtained results, indicating that the catalysts exhibit Tafel slopes that are consistent with or comparable to those reported for similar materials in the existing body of scientific literature.

The stability of the tested materials was evaluated using chronopotentiometry measurements over a duration of 3600 s. The results revealed that almost all the materials, except pure TiO_2 nanotubes, exhibited excellent stability under the applied experimental conditions (see Fig. 17). Chronopotentiometry is a reliable technique

Electrode	b (mV dec^{-1})	References
1T- MoS_2 -GNR	50	35
MoS_2 (1T)	140	36
1T- MoS_2 /CC	55	37
MCM@ MoS_2 -Ni	179	38
Se- MoS_2 -NF	75	39
Zn@ MoS_2	78	40
MoS_2 nanowall	78	41
$\text{Co}_9\text{S}_8/\text{MoS}_2$	118	42
CN/CNL/ MoS_2 /CP(1T/2H)	77	43
Co-BDC/ MoS_2 (1T)	86	44
$\text{MoS}_2/\text{Bi}_2\text{Te}_3/\text{SrTiO}_3$	58	45
Pt@ MoS_2 (1T)	56	46
PtNPs on MoS_2	29	47

Table 4. Literature-based Tafel slope values for MoS_2 -based.

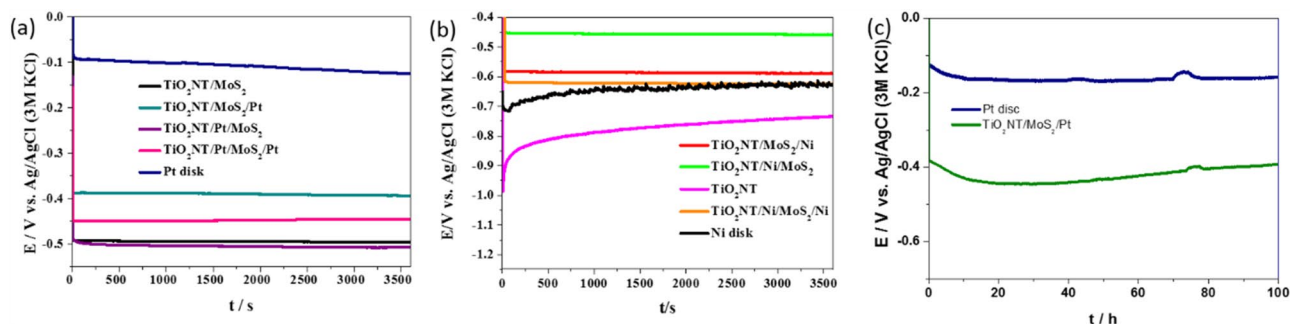


Figure 17. Stability of hybrids $\text{TiO}_2\text{NT}/\text{MoS}_2$ with (a) Pt and (b) Ni at a current density of -10 mA cm^{-2} . (c) Stability measurement for $\text{TiO}_2\text{NT}/\text{MoS}_2/\text{Pt}$ and Pt disk during 100 h.

for assessing the long-term stability of electrocatalytic materials. By applying a constant current (-10 mA cm^{-2}) to the electrodes and monitoring the corresponding potential changes over time, it is possible to evaluate the durability and performance of the catalyst. In this study, except for the pure TiO_2 nanotubes, nearly all materials demonstrated remarkable stability during the 3600-s chronopotentiometry measurements. The absence of significant potential fluctuations or degradation suggests that these materials retained their catalytic activity and structural integrity over an extended period, reinforcing their suitability for practical applications. Material stability is crucial for successful utilization in various electrochemical devices and processes. The observed stability in the chronopotentiometry measurements confirms the robustness and reliability of the tested materials, providing a solid foundation for their potential implementation in real-world applications.

Additionally, stability measurements were conducted at a current density of $-10 \text{ mA}/\text{cm}^2$ for 100 h for both the $\text{TiO}_2\text{NT}/\text{MoS}_2/\text{Pt}$ electrode and, for comparison, the Pt disk electrode. The results indicate minor changes in potential for both the synthesized material and the commercial disk electrode. It can be stated that the materials exhibit stability over time during electrochemical measurements. An unexpected increase in potential was observed around 80 h for both materials (measurements were performed simultaneously using the same instrument, as the potentiostat–galvanostat has multiple measurement channels). Unfortunately, explaining the events after this hour is challenging, and an issue with the measurement setup likely occurred.

Conclusions

In summary, this study investigated the catalytic activity of $\text{TiO}_2\text{NT}/\text{MoS}_2$ hybrids modified with platinum and nickel additives for the hydrogen evolution reaction. The linear sweep voltammograms revealed promising catalytic activity for the hybrids compared to $\text{TiO}_2\text{NT}/\text{MoS}_2$ electrodes without incorporated metals. Although the overpotential values for achieving a current density of $j_{\text{HER}} = 10 \text{ mA cm}^{-2}$ were slightly higher for the hybrids compared to the commercial Pt disk electrode, incorporating a small amount of metal positively influenced the catalytic performance. The Tafel plots provided insights into the kinetic behavior of the electrodes during the HER. The hybrids incorporating metals exhibited lower Tafel slopes, indicating improved catalytic performance compared to pure TiO_2 nanotubes. Notably, the hybrids with nickel additives showed significantly reduced Tafel slopes, approaching the performance level of the commercial Pt disk electrode. This finding highlights the potential of nickel-based hybrids as cost-effective alternatives to platinum-based catalysts. Furthermore, the positioning of the metal within the hybrids played a crucial role in enhancing electrocatalytic activity. Hybrids with the metal located on the surface of MoS_2 demonstrated superior catalytic performance, suggesting the importance of proximity to active sites and facilitating efficient electron transfer. This study emphasizes the improved electrocatalytic performance of $\text{TiO}_2\text{NT}/\text{MoS}_2$ hybrids with metal additives, particularly nickel, and the significance of surface positioning of the metal for enhanced catalytic efficiency. These findings provide valuable insights for designing and developing efficient electrocatalysts, offering cost-effective alternatives to platinum-based catalysts in various electrochemical processes.

Data availability

The datasets generated and/or analyzed during the current study are available in the BRIDGE OF KNOWLEDGE repository (<https://mostwiedzy.pl/pl/open-research-data/xrd-for-molybdenum-sulfide-modified-with-nickel-or-platinum-nanoparticles>, 41501570545750-0), <https://doi.org/10.34808/g88q-cd27>.

Received: 9 April 2024; Accepted: 9 July 2024

Published online: 27 July 2024

References

- Xie, J. & Xie, Y. Transition metal nitrides for electrocatalytic energy conversion: opportunities and challenges. *Chem.–Eur. J.* **22**, 3588–3598 (2016).
- Kumar, S., Kaur, R. & Sharma, S. Recent reports on hydrogen evolution reactions and catalysis. *Results Chem.* **4**, 100613. <https://doi.org/10.1016/j.rechem.2022.100613> (2022).
- Chu, F. *et al.* Nanoscale heterogeneous FeB metallic glass as highly active and stable catalyst for hydrogen evolution. *J. Alloys Compd.* **960**, 170964. <https://doi.org/10.1016/j.jallcom.2023.170964> (2023).

4. Sun, C. *et al.* Atomic-level design of active site on two-dimensional MoS₂ toward efficient hydrogen evolution: experiment, theory, and artificial intelligence modelling. *Adv. Funct. Mater.* **32**, 2206163 (2022).
5. Cao, Y. Roadmap and direction toward high-performance MoS₂ hydrogen evolution catalysts. *ACS Nano* **15**, 11014–11039 (2021).
6. Li, L. *et al.* One-pot synthesis of ultrafine Pt-decorated MoS₂/N-doped carbon composite with sponge-like morphology for efficient hydrogen evolution reaction. *J. Alloys Compd.* **872**, 159562. <https://doi.org/10.1016/j.jallcom.2021.159562> (2021).
7. Li, B. *et al.* Engineering single-layer hollow structure of transition metal dichalcogenides with high 1T-phase purity for hydrogen evolution reaction. *Adv. Mater.* **35**, 2303285 (2023).
8. Wendumu, T. B., Seifert, G., Lorenz, T., Joswig, J.-O. & Enyashin, A. Optical properties of triangular molybdenum disulfide nanoflakes. *J. Phys. Chem. Lett.* **5**, 3636–3640 (2014).
9. Liu, Z. *et al.* General bottom-up colloidal synthesis of nano-monolayer transition-metal dichalcogenides with high 1T'-phase purity. *J. Am. Chem. Soc.* **144**, 4863–4873 (2022).
10. Meng, C. *et al.* Recent modification strategies of MoS₂ for enhanced electrocatalytic hydrogen evolution. *Molecules* **25**, 1136 (2020).
11. Reddy, D. A., Park, H., Hong, S., Kumar, D. P. & Kim, T. K. Hydrazine-assisted formation of ultrathin MoS₂ nanosheets for enhancing their co-catalytic activity in photocatalytic hydrogen evolution. *J. Mater. Chem. A* **5**, 6981–6991 (2017).
12. Zuo, P. *et al.* Metal (Ag, Pt)-MoS₂ hybrids greenly prepared through photochemical reduction of femtosecond laser pulses for SERS and HER. *ACS Sustain. Chem. Eng.* **6**, 7704–7714 (2018).
13. Li, B. *et al.* Pd coated MoS₂ nanoflowers for highly efficient hydrogen evolution reaction under irradiation. *J. Power Sources* **284**, 68–76 (2015).
14. Wang, H. *et al.* Transition-metal doped edge sites in vertically aligned MoS₂ catalysts for enhanced hydrogen evolution. *Nano Res.* **8**, 566–575 (2015).
15. Fu, Y.-G., Liu, H.-Q., Liu, C. & Lü, Q.-F. Ultralight porous carbon loaded Co-doped MoS₂ as an efficient electrocatalyst for hydrogen evolution reaction in acidic and alkaline media. *J. Alloys Compd.* **967**, 171748. <https://doi.org/10.1016/j.jallcom.2023.171748> (2023).
16. Luo, Z. *et al.* Chemically activating MoS₂ via spontaneous atomic palladium interfacial doping towards efficient hydrogen evolution. *Nat. Commun.* **9**, 2120 (2018).
17. Bar-Ziv, R. *et al.* Au-MoS₂ hybrids as hydrogen evolution electrocatalysts. *ACS Appl. Energy Mater.* **2**, 6043–6050 (2019).
18. Wang, K. *et al.* Crystalline Ru(0.33) Se nanoparticles-decorated TiO₂ nanotube arrays for enhanced hydrogen evolution reaction. *Small* **14**, e1802132. <https://doi.org/10.1002/smll.201802132> (2018).
19. Paramasivam, I., Jha, H., Liu, N. & Schmuki, P. J. S. A review of photocatalysis using self-organized TiO₂ nanotubes and other ordered oxide nanostructures. *small* **8**, 3073–3103 (2012).
20. Szkoda, M. *et al.* Ti-Fe₂O₃/In₂O₃ as photoactive material: The role of the substrate in photoelectrochemical water oxidation. *J. Alloys Compd.* **960**, 170924 (2023).
21. Szkoda, M., Ilnicka, A., Skorupska, M., Wysokowski, M. & Lukaszewicz, J. P. J. S. R. Modification of TiO₂ nanotubes by graphene-strontium and cobalt molybdate perovskite for efficient hydrogen evolution reaction in acidic medium. *Sci. Rep.* **12**, 22577 (2022).
22. Siuzdak, K., Szkoda, M., Sawczak, M. & Lisowska-Oleksiak, A. Novel nitrogen precursors for electrochemically driven doping of titania nanotubes exhibiting enhanced photoactivity. *New J. Chem.* **39**, 2741–2751 (2015).
23. Szkoda, M., Trzciński, K., Lisowska-Oleksiak, A. & Siuzdak, K. J. A. S. S. Electrochemical and photoelectrochemical properties of the interface between titania nanotubes covered by conducting polymer in aqueous electrolyte by conducting polymer in aqueous electrolytes—The effect of various geometry and electrolytes concentration. *Appl. Surf. Sci.* **448**, 309–319 (2018).
24. Siuzdak, K. *et al.* Ordered titania nanotubes layer selectively annealed by laser beam for high contrast electrochromic switching. *Thin Solid Films* **659**, 48–56 (2018).
25. Trzciński, K., Szkoda, M., Siuzdak, K., Sawczak, M. & Lisowska-Oleksiak, A. J. E. A. Electrochemical and photoelectrochemical characterization of photoanodes based on titania nanotubes modified by a BiVO₄ thin film and gold nanoparticles. *Electrochim. Acta* **222**, 421–428 (2016).
26. Børresen, B., Hagen, G. & Tunold, R. Hydrogen evolution on Ru_xTi_{1-x}O₂ in 0.5 M H₂SO₄. *Electrochim. Acta* **47**, 1819–1827 (2002).
27. Szkoda, M., Lisowska-Oleksiak, A. & Siuzdak, K. Optimization of boron-doping process of titania nanotubes via electrochemical method toward enhanced photoactivity. *J. Solid State Electrochem.* **20**, 1765–1774 (2016).
28. Eda, G. *et al.* Photoluminescence from chemically exfoliated MoS₂. *Nano Lett.* **11**, 5111–5116 (2011).
29. Baltrusaitis, J. *et al.* Generalized molybdenum oxide surface chemical state XPS determination via informed amorphous sample model. *Appl. Surf. Sci.* **326**, 151–161 (2015).
30. Fantauzzi, M., Elsener, B., Atzei, D., Rigoldi, A. & Rossi, A. Exploiting XPS for the identification of sulfides and polysulfides. *RSC Adv.* **5**, 75953–75963 (2015).
31. Sreelakshmi, V., Anu Kaliani, A. & Jithin, M. Photochromic and hydrophilic self-cleaning nature of MoO₃ thin films. *J. Mater. Sci. Mater. Electron.* **33**, 1–13 (2022).
32. Biesinger, M. C. *et al.* Resolving surface chemical states in XPS analysis of first row transition metals, oxides and hydroxides: Cr, Mn, Fe, Co and Ni. *Appl. Surf. Sci.* **257**, 2717–2730 (2011).
33. Biesinger, M. C., Payne, B. P., Lau, L. W., Gerson, A. & Smart, R. S. C. X-ray photoelectron spectroscopic chemical state quantification of mixed nickel metal, oxide and hydroxide systems. *Surf. Interface Anal.: Int. J. Devot. Dev. Appl. Tech. Anal. Surf. Interfaces Thin Films* **41**, 324–332 (2009).
34. Wagner, C. D. *et al.* (Version, 2003).
35. Ekspong, J. *et al.* Stable sulfur-intercalated 1T' MoS₂ on graphitic nanoribbons as hydrogen evolution electrocatalyst. *Adv. Funct. Mater.* **28**, 1802744 (2018).
36. Tan, C. *et al.* Preparation of high-percentage 1T-phase transition metal dichalcogenide nanodots for electrochemical hydrogen evolution. *Adv. Mater.* **30**, 1705509 (2018).
37. Liu, Z. *et al.* Vertical nanosheet array of 1T phase MoS₂ for efficient and stable hydrogen evolution. *Appl. Catal. B: Environ.* **246**, 296–302 (2019).
38. Zhang, H., Yu, L., Chen, T., Zhou, W. & Lou, X. W. Surface modulation of hierarchical MoS₂ nanosheets by Ni single atoms for enhanced electrocatalytic hydrogen evolution. *Adv. Funct. Mater.* **28**, 1807086 (2018).
39. Zheng, Z. *et al.* Boosting hydrogen evolution on MoS₂ via co-confining selenium in surface and cobalt in inner layer. *Nat. Commun.* **11**, 3315. <https://doi.org/10.1038/s41467-020-17199-0> (2020).
40. Wu, W. *et al.* Activation of MoS₂ basal planes for hydrogen evolution by zinc. *Angew. Chem. Int. Edit.* **58**, 2029–2033 (2019).
41. Xie, J. *et al.* Defect-rich MoS₂ nanowall catalyst for efficient hydrogen evolution reaction. *Nano Res.* **10**, 1178–1188 (2017).
42. Chen, T.-T., Wang, R., Li, L.-K., Li, Z.-J. & Zang, S.-Q. MOF-derived Co₉S₈/MoS₂ embedded in tri-doped carbon hybrids for efficient electrocatalytic hydrogen evolution. *J. Energy Chem.* **44**, 90–96 (2020).
43. Dong, J. *et al.* In-situ formation of unsaturated defect sites on converted CoNi alloy/Co-Ni LDH to activate MoS₂ nanosheets for pH-universal hydrogen evolution reaction. *Chem. Eng. J.* **412**, 128556 (2021).
44. Zhu, D., Liu, J., Zhao, Y., Zheng, Y. & Qiao, S. Z. Engineering 2D metal-organic framework/MoS₂ interface for enhanced alkaline hydrogen evolution. *Small* **15**, 1805511 (2019).
45. Li, G. *et al.* MoS₂ on topological insulator Bi₂Te₃ thin films: Activation of the basal plane for hydrogen reduction. *J. Energy Chem.* **62**, 516–522 (2021).

46. Li, Y. *et al.* Synergistic Pt doping and phase conversion engineering in two-dimensional MoS₂ for efficient hydrogen evolution. *Nano Energy* **84**, 105898 (2021).
47. Li, Y. *et al.* Highly dispersed Pt nanoparticles on 2D MoS₂ nanosheets for efficient and stable hydrogen evolution reaction. *J. Mater. Chem. A* **10**, 5273–5279 (2022).

Acknowledgements

The research leading to these results has received funding from the Norway Grants 2014-2021 via the National Centre for Research and Development. This work was carried out as a result of the research project no. NOR/SGS/IL-HYDROGEN/0202/2020-00. Financial support of these studies from Gdańsk University of Technology by the DEC- 2/1/2022/IDUB/III.4c/Tc Technetium Talent Management Grants.

Author contributions

M.Sz.: Conceptualization, Methodology, Investigation, Formal analysis, Visualization, Writing—original draft, Writing—review and editing, Supervision. D.R.: Investigation, Formal analysis, Visualization, Writing—original draft. M.Sk.: Investigation, Formal analysis. R.G.: Investigation, Formal analysis, Technical help. A.I.: Methodology, Investigation, Formal analysis, Visualization, Writing—original draf, Writing—review and editing, Project administration, Funding acquisition.

Competing interests

The authors declare no competing interests.

Additional information

Correspondence and requests for materials should be addressed to M.S.

Reprints and permissions information is available at www.nature.com/reprints.

Publisher's note Springer Nature remains neutral with regard to jurisdictional claims in published maps and institutional affiliations.



Open Access This article is licensed under a Creative Commons Attribution-NonCommercial-NoDerivatives 4.0 International License, which permits any non-commercial use, sharing, distribution and reproduction in any medium or format, as long as you give appropriate credit to the original author(s) and the source, provide a link to the Creative Commons licence, and indicate if you modified the licensed material. You do not have permission under this licence to share adapted material derived from this article or parts of it. The images or other third party material in this article are included in the article's Creative Commons licence, unless indicated otherwise in a credit line to the material. If material is not included in the article's Creative Commons licence and your intended use is not permitted by statutory regulation or exceeds the permitted use, you will need to obtain permission directly from the copyright holder. To view a copy of this licence, visit <http://creativecommons.org/licenses/by-nc-nd/4.0/>.

© The Author(s) 2024